Containment and Consensus-based Distributed Coordination Control to Achieve Bounded Voltage and Precise Reactive Power Sharing in Islanded AC Microgrids

Renke Han, *Student Member, IEEE*, Lexuan Meng, *Member, IEEE*, Giancarlo Ferrari-Trecate, *Senior Member, IEEE*, Ernane Antonio Alves Coelho, *Member, IEEE*, Juan C. Vasquez, *Senior Member, IEEE*, Josep M. Guerrero, *Fellow, IEEE*

***Abstract*—This paper presents a novel distributed approach to achieve both bounded voltage and accurate reactive power sharing regulation in AC microgrid. The coupling/trade-off effects between bus voltages and reactive power sharing regulation are first analyzed in detail to provide a guideline for coordinated control design. Furthermore, a containment and consensus-based distributed coordination controller is proposed, by which the bus voltage magnitudes can be bounded within a reasonable range, instead of only controlling average voltage value. Further, the accurate reactive power sharing between distributed generators can be achieved simultaneously. Then, a detailed small-signal model is developed to analyze the stability of the system and the sensitivity of different parameters. Experimental results are presented and compared, where the controller performance, robust performance under communication failure and plug-and-play operation are successfully verified.**

***Index Terms*—Containment algorithm, consensus algorithm, coordinated control, bounded voltage, reactive power sharing, microgrid.**

I. Introduction

The microgrid (MG) concept provides a promising mean of integrating large amount of distributed generators (DGs) into the power grid and improving reliability [1]. Based on the MG concept, hierarchical control architecture, which was commonly applied in power systems, has been adopted and modified to coordinate different control objectives and to standardize the MG operation [2], [3]. Typically, the primary level deals with the voltage/current regulation and power sharing local control. The secondary level is used to restore the system frequency and voltage to nominal values, regardless of load changes. The tertiary level deals with the energy management and optimization issues.

For the primary and secondary levels, one of main challenges is to achieve the coordination between reactive power sharing and output voltage magnitudes regulation. The reactive power-to-voltage (*Q-V*) droop control [4] is applied to achieve reactive power sharing in a decentralized manner. However, the *Q-V* droop control is very sensitive to line impedance differences thus producing inaccurate reactive power sharing and deviating the voltage excessively when researchers try to correct it by increasing the droop coefficient value [5]. In [6], the reactive power sharing problem is analyzed and a two-step estimation method is proposed to calculate the local reactive load, based on which the droop gain is adjusted accordingly to improve the reactive power sharing. Both the effects from local loads and line impedances are considered to improve the power sharing performance. However, the load information should be identified in advance. Then, with a centralized energy management system, a dynamic virtual impedance is proposed in order to satisfy the reactive power sharing requirements based on the different load conditions [7]. However, the load information is also required by the centralized controller, which limits the expandability of the proposed controller. In addition, the centralized controller can cause the single point of failure. In [8], according to the electrical topology of the MG, the relationship between active/reactive load changes and reactive power sharing error is analyzed, and a genetic algorithm is applied to optimize the virtual impedance, in order achieve reactive power sharing. However, when the topology of MG is changed, the whole optimization problem needs to be reformulated. Notice that all the aforementioned controllers are focusing just on the reactive power sharing, while the problem of voltage recovery is not considered at the same time.

Recently, distributed control algorithms [9]-[13] are coming up to stage finding their applications in the MG area [14]-[21]. A distributed method is proposed in [14] to achieve reactive power sharing through acquiring the average value of reactive power. Similarly, in [15], considering the converters parameters related to the power limit and maximum active power capability, a reactive power sharing algorithm is developed. However, for the above two kinds of controllers, each distributed controller needs to know the output reactive power and output voltage magnitudes of all the other DGs in the MG. Thus, if one DG fails, the operating DG number should be updated for all the other controllers, which limits the flexibility and robustness of the system. Furthermore, in [15], the voltage regulation is not considered, which may result in considerable voltage deviations. On the other hand, based on the distributed leader-following tracking algorithm [9], another work [16] proposes a secondary voltage tracking strategy by using the feedback linearization method, achieving the output voltage magnitudes tracking the leader. However, the problem of reactive power sharing is not considered during the controller design process. In another work [17], in order to evaluate the issues between accurate reactive power sharing and voltage magnitude regulation, a simple trade-off analysis is proposed for the two control objectives within the secondary control level. Then, an averaging-based method [13] has been applied to achieve reactive power sharing and to keep the average voltage value equal to the nominal value. However, in this work only the average value of all output voltage magnitudes is regulated, being possible large local voltage deviations.

Alternatively, in [19], a droop-free distributed method is proposed to achieve power sharing and to fix the average output voltage to the nominal value. However, the system cannot be operated in practical applications without the use of

droop control when the communication system is disabled or presents a global failure. Furthermore, only controlling the average voltage value is not enough for some operation conditions. For example, when one or several DGs are disconnected from the MG or the difference among output line impedances are large, the voltage at some buses deviate out from the allowed limit, which can affect the power quality of the system, even though the average voltage value is kept at the nominal value [22]. Compared with the voltage deviation standard for electrical distribution networks, e.g. IEEE 1547, the voltage deviations in an islanded MG should be smaller to guarantee stable of the MG. Accordingly, the existing literature only focus on regulating the average value of voltage magnitudes rather than bounding all bus voltage magnitudes in a reasonable range.

Thus, instead of only controlling the average voltage value, a more flexible control strategy is required to bound all bus voltage magnitudes into a reasonable range, and to achieve accurate reactive power simultaneously. In more serious conditions, to guarantee the bus voltages bounded and to provide voltage support for the system stability, the performance of reactive power sharing should be compromised to some extent. In addition, the coupling and trade-off effects between critical system parameters, including droop gains, line impedances, voltage magnitude deviations, and reactive power sharing errors should be analyzed in detail by considering different conditions.

To solve the abovementioned critical issues, a containment-based controller [23] is identified and considered as a reasonable and flexible approach. It can bound objects within a convex range, while maintaining the distributed fashion, which make it highly suitable for DG-based MG applications.

In this paper, there are four main technical contributions. First, coupling and trade-off effects between different control parameters and objectives are analyzed within primary and secondary control level. Second, a fully distributed coordination control scheme including containment-based and consensus-based algorithms is proposed realizing a well coordination between bounded bus voltage and accurate reactive power sharing. Third, the small-signal model is derived for system stability analysis and control parameter design. Finally, experimental results including control and robust performance comparison, especially under communication links failure and plug-and-play conditions are shown to prove high resiliency of the proposed controller.

The paper is organized as follows. In Section II, the coupling and trade-off effects within the hierarchical control structure are analyzed. In Section III, containment and consensus-based distributed coordination control strategy is introduced in detail. In Section IV, the small-signal model and its stability analysis are provided. In Section V, experimental results are presented to prove the effectiveness of proposed controller. Finally, the paper is concluded in Section VI.

II. Coupling and Trade-off Analysis within the Hierarchical Control

This Section gives the coupling analysis among *Q-V* droop gains, line impedance differences, reactive power sharing errors, and relative deviations of voltage magnitudes. Then, the trade-off effects between the accurate reactive power sharing regulation and voltages regulation are analyzed.

A. Coupling Analysis in the Primary Control Level

The simplified islanded MG for analysis purposes is shown in Fig. 1, including two DGs, two local loads, and one common load.

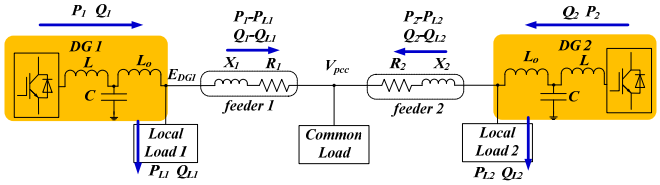

Fig. 1. Simplified model of the microgrid

During the islanded operation, DG units are operated under conventional *Q-V* droop control, defined as:

$$E_{DGi} = E^* - n_i Q_i \tag{1}$$

where E_{DGi} is the reference voltage for the inner control loop, E^* is the voltage magnitude reference of droop control, n_i is the *Q-V* droop gain, and Q_i is the output reactive power.

In Fig. 1, according to the line impedances, the voltage drop can be calculated as [24]:

$$E_{DGi} - V_{pcc} = \frac{R_i(P_i - P_{Li}) + X_i(Q_i - Q_{Li})}{V^*} \tag{2}$$

where V^* is the nominal voltage according to the system requirement, R_i and X_i are the line impedance, P_i and Q_i are the output active and reactive powers, and P_{Li} and Q_{Li} are the local active and reactive powers for *i*-th DG.

From (1) and (2), the coupling effects of droop gains and line impedance ratios on reactive power sharing error and voltage magnitude deviations can be analyzed by using the control variate method, shown in Fig. 2. For convenience, same droop gains, $n_1=n_2=n$, are assumed in this analysis. Note that in this figure logarithm horizontal *x*-axis is used to show clearly the trends.

Fig. 2(a.1) shows the effect of absolute *Q-V* droop gains and the ratio of line impedances on reactive power sharing error. To be more specific, Fig. 2(a.2) is given indicating the relationship between absolute *Q-V* droop gains and reactive power sharing error. It is shown that the reactive power sharing error can be effectively reduced by increasing droop gains regardless of line impedance ratios. Fig. 2(a.3) shows the relationship between the line impedance ratios and the reactive power sharing error. It is shown that with the increasing of line impedance ratios, the reactive power sharing error is increased, while larger absolute *Q-V* droop gain can reduce this error.

From the other standpoint, Fig. 2(b.1) shows the effect of absolute *Q-V* droop gains and the line impedance ratios on relative deviations of output voltage magnitudes of DG units. As shown in Fig. 2(b.2), both smaller and larger droop gains can help to reduce the relative deviations of voltage magnitudes. Here, it is emphasized that due to the feature of *Q-V* droop control, the voltage magnitudes are always deviated from the nominal value and in this subsection, the relative deviations between voltage magnitudes of only two DGs are discussed to make the explanation easier. The voltage restoration will be discussed in subsection II-B. In addition, there exist several peak values for different line impedances conditions shown in Fig. 2(b.2), which is also proven by Fig. 2(b.3). Thus, by combining the results with those from Fig. 2(a.1)-(a.3), the relatively larger droop gains within the stability range can relieve the reactive power sharing error and voltage magnitude relative deviations effectively simultaneous.

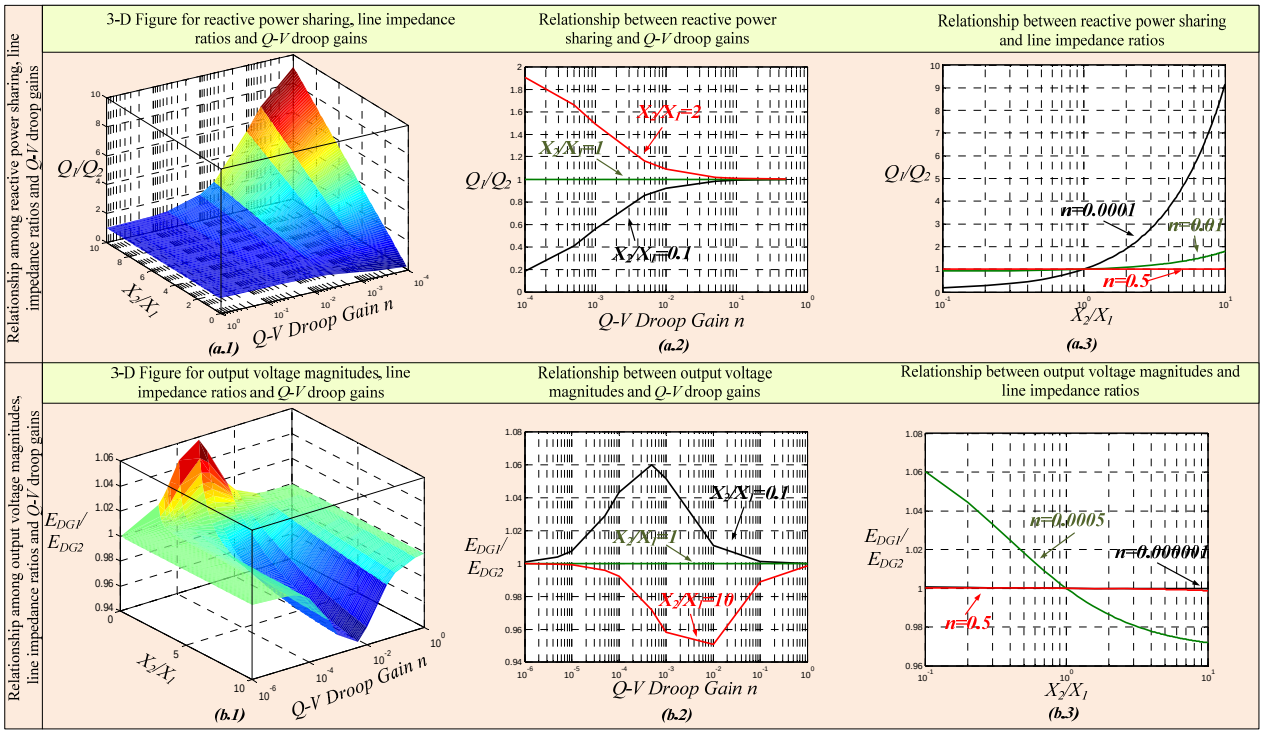

Fig. 2. Coupling analysis results.

Based on the above analyses, the following four main conclusions can be obtained:

1) Both larger and smaller droop gains can help decreasing the relative deviations of output voltage magnitudes to reduce the reactive circuit current.

2) Larger droop gains can weaken the effect of line impedance differences and decrease the reactive power sharing errors.

3) Based on 1) and 2), larger droop gains are more suitable to decrease two errors under the assumption that the droop gain can satisfy the stability requirements

4) The absolute droop gains and line impedances have decisive influence over the relative voltage deviations and reactive power sharing errors rather than the relative ratios.

B. Trade-off Analysis between Voltage Magnitude Regulation and Reactive Power Sharing in the Secondary Control Level

Due to the features of above analyses in the primary level, two control objectives should be achieved: voltage recovery and accurate reactive power sharing in the secondary level. In this Subsection, it is analyzed that trade-off effects always exist between the two objectives with different line impedances from DG units.

To analyze the trade-off effects between voltage regulation and reactive power sharing regulation under different conditions, Figs. 3-6 are depicted, in which black lines denote the condition before secondary control regulation, red lines stand for the condition after secondary control regulation. The analyses are divided in two parts. Figs. 3-4 are only considering the effect of voltage regulation, while Figs. 5-6 are only investigating the effect of reactive power sharing regulation.

Fig. 3 gives the condition with smaller Q-V droop gain and larger line impedance difference, after regulating the voltage magnitude to the nominal value, Q_1 becomes much smaller and Q_2 becomes much larger than before. If larger Q-V droop gain and smaller line impedance difference are considered, as shown in Fig. 4, after voltage regulation, the deviation between Q_1 and Q_2 also becomes larger. Thus, no matter what kind of parameter conditions are chosen in the system, the trade-off effect is observable.

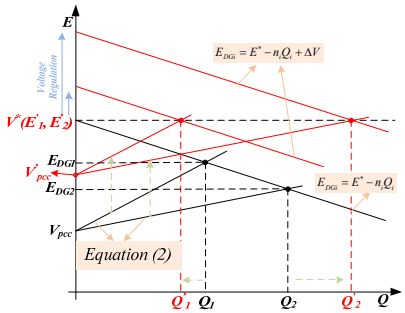

Fig. 3. Voltage magnitudes regulation control for two parallel DGs with smaller droop gain and larger line impedance difference.

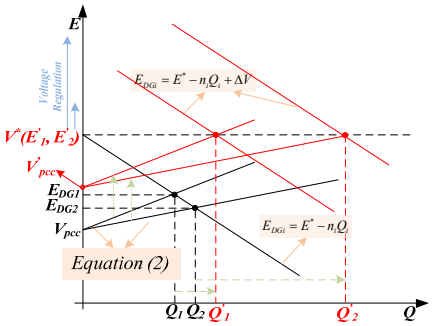

Fig. 4. Voltage magnitudes regulation control for two parallel DGs with larger droop gain and smaller line impedance difference.

In Fig. 5, a smaller Q-V droop gain and a larger line impedance difference condition are assumed, after reactive power sharing regulation, the voltage deviation between two

DGs is enlarged. In Fig. 6, a relative larger *Q-V* droop gain and a smaller line impedance difference are assumed as another condition, after the reactive power sharing regulation, the voltage deviation from two DGs is almost not changed.

Thus, regulating voltage magnitudes to nominal value can cause larger deviation of reactive power sharing. By comparison, reactive power sharing regulation can cause relative little effects in voltage magnitude deviations. Based on above discussions, a reasonable operation strategy is to ensure accurate reactive power sharing regardless of relative voltage deviations between buses, but necessarily, bounding voltage magnitudes within a reasonable range defined by standards to guarantee the stability and power quality.

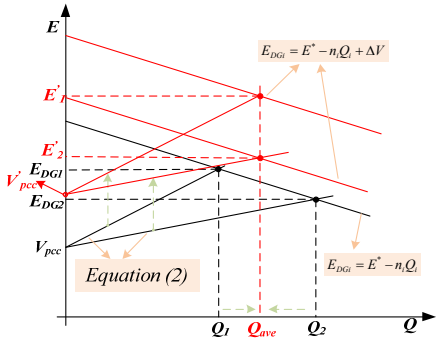

Fig. 5. Reactive power sharing regulation control for two parallel DGs with smaller droop gain and larger line impedance differences

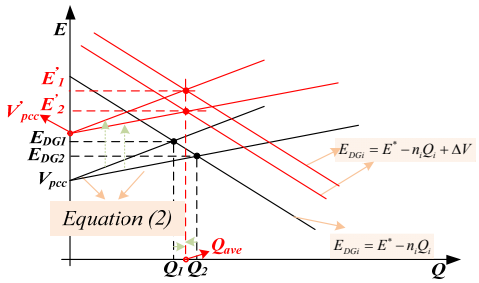

Fig. 6. Reactive power sharing regulation control for two parallel DGs with larger droop gain and smaller line impedance differences

III. Proposed Distributed Coordination Control for Bounding Voltage Deviations and Reactive Power Sharing

This Section explains the proposed distributed coordination control in detail. Comparing with the algorithms presented in the literature [14], [17], [19], the proposed algorithm can achieve the controllability of all the bus voltages instead of only controlling the average value of them. A containment-based voltage controller is firstly proposed to bound all the bus voltages into allowed range, which can guarantee the power quality of the system even under worst conditions, especially for the system with the larger line impedance differences or the system with necessary plug-and-play operations. Compared with the proposed method, the conventional average value based controller may result in over-/under-voltage ranges in some of the buses although the average value of all bus voltages can be kept at nominal value. At the same time, a consensus-based reactive power controller is also involved in the proposed control algorithm to achieve proper reactive power sharing. Thus, the proposed two controllers can achieve the coordinated control including the global bounded bus voltages and reactive power sharing simultaneously. A hierarchical control structure can be formulated to integrate of multiple functions seamlessly.

A. Definitions and Notations

For the control system with n distributed controllers, a controller is called *leader* if it only provides information to its communication neighbors and does not receive information. A controller is called *follower* if it can receive information from one or more neighbors through communication topology. Let N_i denote the set of i_{th}-controller neighbors chosen from followers, and R_i denote the set of leaders, which can send its information to i_{th}-agent directly. The definition above is applied to containment-based voltage controller. At the same time, the consensus-based reactive power controller only uses the neighbors' information without the leaders' information.

Let C be a set in a real vector space $V \subseteq R^p$. The set C is called convex if, for any x and y in C, the point $(1-z)x+zy$ is also in C for any $z \in [0,1]$. The convex hull for a set of points $X=\{x_1,\ldots,x_q\}$ in V is the minimal convex set containing all points in X. Let $Co(X)$ denote the convex hull of X. In particular, when $V \subseteq R$, $Co(X)=\{x \mid x \in [\min x_i, \max x_i]\}$ which will be used in following. In addition, define vector $Z \in R^n$, then $diag(Z) \in R^{n\times n}$ as the diagonal matrix whose diagonal elements are the elements in vector Z. I_n is the unit matrix and 0_n is the zero $n\times n$ matrix.

For consensus-based control, an adjacency matrix is defined as $A=[a_{ij}] \in R^{n\times n}$ with $a_{ij}>0$ if node i can receive information from node j otherwise $a_{ij}=0$. The Laplacian matrix is defined as $L_Q=[l_{ij}] \in R^{n\times n}$ with $l_{ii}=\sum_{j=1}^{n} a_{ij}$ and $l_{ij}=-a_{ij}$, $i \neq j$.

For containment-based control, the range is formed by two leaders which are called the lower and upper voltage boundaries respectively. Thus another adjacency matrix is defined as $B=[b_{il}] \in R^{n\times 2}$ with $b_{il}=1$ if node i can receive information from one of the two leaders otherwise $b_{il}=0$, in which l represents the label of two leaders; Another Laplacian matrix is defined as $L_E=[l_{ij}] \in R^{n\times(n+2)}$ with $l_{ii}=\sum_{j=1}^{n} a_{ij}+\sum_{l=n+1}^{n+2} b_{il}$ for other rows, when $j<n$, $l_{ij}=-a_{ij}$, otherwise when $j>n$, $l_{ij}=-b_{ij}$.

B. Proposed Coordination Controller

The containment-based controller generates a correction term e_{Ei} for each DG to keep the voltage within a range which is as convex hull. The controller expression is defined as:

$$\dot{e}_{Ei}=-\sum_{j\in N_i} a_{ij}\left(E_{DGi}-E_{DGj}\right)-\sum_{l\in R_i} b_{il}\left(E_{DGi}-E_l\right) \tag{3}$$

where E_{DGi} and E_{DGj} are the voltage magnitudes of i-th DG and j-th DG respectively, E_l is the voltage leader which can be either upper boundary E_{Ubou} or lower boundary E_{Lbou}.

Eq. (3) can be written into matrix form as:

$$\dot{e}_E=-L_E\mathbf{E} \tag{4}$$

where $E_{DG}=[E_{DG1}, \cdots E_{DGn}]^T$, $E_{leader}=[E_{Ubou} \quad E_{Lbou}]^T$,

$\mathbf{E}=\left[E_{DG}^T \quad E_{leader}^T\right]^T$, $e_E=[e_{E1} \cdots e_{En}]^T$.

Then the error $\dot{e}_E$ is fed into a *PI* controller.

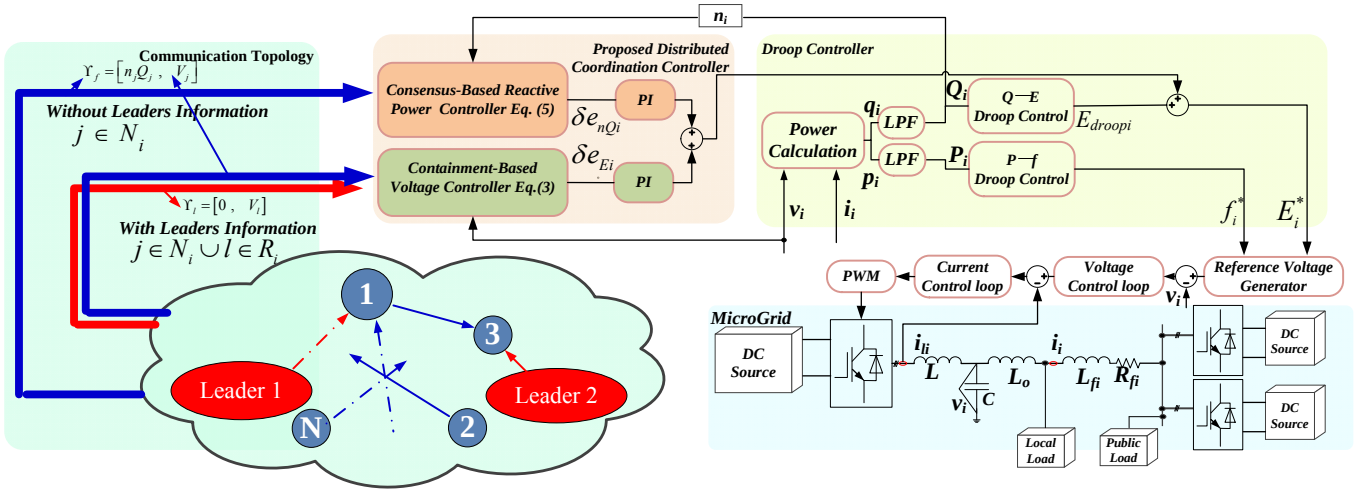

Fig. 7. Configuration of the Containment-based and Consensus-based Distributed Coordination Controller.

Consensus-based reactive power controller is defined as:

$$\dot{e}_{nQi} = -\sum_{j\in N_i} a_{ij}\left(n_i Q_i - n_j Q_j\right) \tag{5}$$

where n_i and n_j are the reactive power droop gains, Q_i and Q_j are the output reactive for i-th DG and j-th DG.

(5) can be written into matrix form as:

$$\dot{e}_{nQ} = -L_Q N Q \tag{6}$$

where $N = diag\left\{\left[n_1, \ \cdots \ n_n\right]^T\right\}$, $e_{nQ} = \left[e_{nQ1} \ \cdots \ e_{nQn}\right]^T$.

Then the error $\dot{e}_{nQ}$ is fed into another *PI* controller.

The configuration of the proposed controller is shown in Fig. 7, including the containment-based voltage controller and the consensus-based reactive power controller. The information format from DGs (followers) is defined as $\Upsilon_{fj} = \left[n_j Q_j, \ V_j\right]$, and the information format from the *leader* is defined as $\Upsilon_l = \left[0, \ E_l\right]$.

C. Different Work Conditions

The proposed algorithms are based on the hierarchical structure, which consists of primary, secondary and tertiary levels. In the primary level, the stability can be guaranteed by the conventional droop controller. The proposed two controllers are implemented in the secondary level, corresponding to two critical operation conditions.

Condition 1: Under this condition, DGs have enough power capacity to support voltage and reactive power regulations. The containment-based controller guarantees that all the bus voltages are kept within a prescribed range defined by standards, while consensus-based controller realizes proportional reactive power sharing by all the DGs at the same time.

Condition 2: Under this condition, all the bus voltages are controlled to be maintained within a dynamic boundary which could be adapted based on the command from the higher control level. Even though the voltage boundary may change, the total reactive power is proportional shared among DGs. It is worth saying that the principle about how to change the voltage boundary is out of the scope of this paper, which should be designed in the tertiary level to achieve power management operation.

Notice that, under both work conditions, the two controllers are activated at the same time. The bounded voltage deviations and precise reactive power sharing can be achieved simultaneously. Both the work conditions have been tested in Section V-A.

IV. Small-Signal Stability Analysis

This Section develops the small-signal model for stability analysis and parameters design purposes. The model includes the proposed containment-based voltage controller, consensus-based reactive power controller, active and reactive power calculation, low-pass filter and droop controller. The whole model is based on the synchronous reference frame.

A. Small-Signal Model for Proposed Controllers

For the containment-based voltage controller shown in (4), the small signal model is expressed as

$$\Delta\dot{e}_E = -L_E^{'}\Delta E_{DG} \tag{7}$$

where $L_E^{'}$ is the matrix which deletes the last two columns of matrix L_E neglecting the dynamic of leaders, $\Delta e_E = \left[\Delta e_{E1} \ \cdots \ \Delta e_{En}\right]^T$, $\Delta E_{DG} = \left[\Delta E_{DG1} \ \cdots \ \Delta E_{DGn}\right]^T$.

For the consensus-based reactive power controller in (6), the small signal model is expressed as

$$\Delta\dot{e}_{nQ} = -L_Q N \Delta Q \tag{8}$$

where $\Delta e_{nQ} = \left[\Delta e_{nQ1} \ \cdots \ \Delta e_{nQn}\right]^T$, $\Delta Q = \left[\Delta Q_1 \ \cdots \ \Delta Q_n\right]^T$.

Considering the dynamic of voltage changes, by adding a voltage disturbance term $\dot{E}_{DG}$ in left part of (1), then it can be rewritten as:

$$\dot{E}_{DG} = E^* - E_{DG} - NQ \tag{9}$$

which can be seen as the dynamic of the primary level control.

As explained above, the two proposed controllers should provide control signals added into (9) through *PI* controllers. Thus, the system can be written as:

$$\Delta\dot{E}_{DG} = -\Delta E_{DG} - N\Delta Q - K_{pQ}L_Q N\Delta Q - K_{pE}L_E^{'}\Delta E_{DG} + K_{iQ}\Delta e_{nQ} + K_{iE}\Delta e_E \tag{10}$$

where $K_{pQ} = diag\left(\left[k_{pQ1} \ \cdots \ k_{pQn}\right]^T\right)$ corresponds to the proportional parameters, $K_{iQ} = diag\left(\left[k_{iQ1} \ \cdots \ k_{iQn}\right]^T\right)$ to the integral parameters of the *PI* controllers for the consensus-

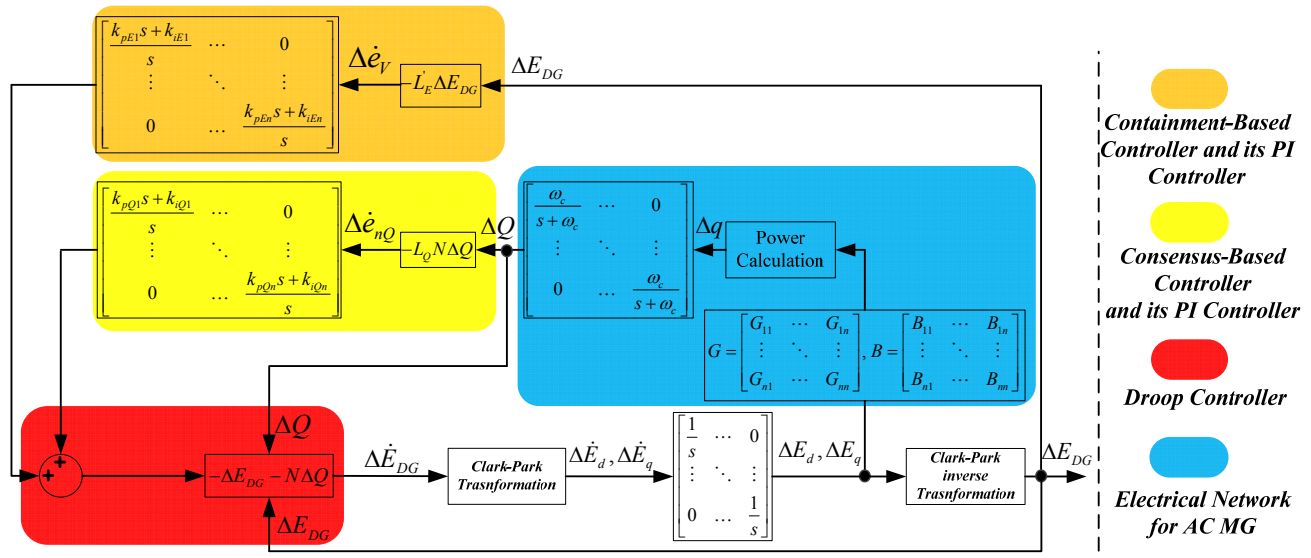

Fig. 8. Small signal model diagram for the whole system.

based reactive power controller, $K_{pE}=diag\left(\left[k_{pE1}\ \cdots\ k_{pEn}\right]^T\right)$ to the proportional parameters and $K_{iE}=diag\left(\left[k_{iE1}\ \cdots\ k_{iEn}\right]^T\right)$ to the integral parameters of the *PI* controller for the containment-based voltage controller.

Due to the low-pass filter effect, the small-signal model of output reactive power Q_i can be written as

$$\Delta\dot{Q}=-\omega_c\Delta Q+\omega_c\Delta q \tag{11}$$

where ω_c is the cut-off frequency of low-pass filter and the instant output reactive power is $\Delta q=\left[\Delta q_1\ \cdots\ \Delta q_n\right]^T$.

Considering synchronous reference frame for the *i-th* DG, the vector voltage $\vec{E}_{DGi}$ can be written as

$$\vec{E}_{DGi}=E_{di}+jE_{qi} \tag{12}$$

where, $E_{di}=E_{DGi}\cos\delta_i, E_{qi}=E_{DGi}\cos\delta_i, \delta_i=\arctan\left(E_{di}/E_{qi}\right)$.

Linearizing (12) of δ_i, we can get

$$\Delta\delta_i=\left(\partial\delta_i/\partial E_{di}\right)\Delta E_{di}+\left(\partial\delta_i/\partial E_{qi}\right)\Delta E_{qi}=m_{di}\Delta E_{di}+m_{qi}\Delta E_{qi} \tag{13}$$

where $m_{di}=-E_{qi}/\left(E_{di}^2+E_{qi}^2\right), m_{qi}=E_{di}/\left(E_{di}^2+E_{qi}^2\right)$.

Since $\Delta\omega_i(s)=s\Delta\delta_i(s)$, (13) can be rewritten as

$$\Delta\omega_i=m_{di}\Delta\dot{E}_{di}+m_{qi}\Delta\dot{E}_{qi} \tag{14}$$

Considering that $E_{DGi}=\left|\vec{E}_{DGi}\right|=\sqrt{E_{di}^2+E_{qi}^2}$, it can be linearized as

$$\Delta E_{DGi}=n_{di}\Delta E_{di}+n_{qi}\Delta E_{qi} \tag{15}$$

where $n_{di}=E_{di}/\sqrt{E_{di}^2+E_{qi}^2}$, $n_{qi}=E_{qi}/\sqrt{E_{di}^2+E_{qi}^2}$.

It follows that

$$\Delta\dot{E}_{DGi}=n_{di}\Delta\dot{E}_{di}+n_{qi}\Delta\dot{E}_{qi} \tag{16}$$

Thus, from the equation set consisted of (14), (16) for variables $\Delta\dot{E}_{di}$ and $\Delta\dot{E}_{qi}$, we have

$$\begin{cases}\Delta\dot{E}_{di}=m_{1i}\Delta\omega+m_{2i}\Delta\dot{E}_{DGi}\\ \Delta\dot{E}_{qi}=m_{3i}\Delta\omega+m_{4i}\Delta\dot{E}_{DGi}\end{cases} \tag{17}$$

where $m_{1i}=n_{qi}/\left(m_{di}n_{qi}-m_{qi}n_{di}\right)$, $m_{2i}=-m_{qi}/\left(m_{di}n_{qi}-m_{qi}n_{di}\right)$,

$m_{3i}=n_{di}/\left(m_{qi}n_{di}-m_{di}n_{qi}\right)$, $m_{4i}=-m_{di}/\left(m_{qi}n_{di}-m_{di}n_{qi}\right)$.

Substituting (10) and (15) into (17) and writing into matrix form as

$$\begin{cases}\Delta\dot{E}_d=M_1\Delta\omega+A_1N_d\Delta E_d+A_1N_q\Delta E_q+A_2\Delta Q+M_2K_{iE}\Delta e_E+M_2K_{iQ}\Delta e_{nQ}\\ \Delta\dot{E}_q=M_3\Delta\omega+B_1N_d\Delta E_d+B_1N_q\Delta E_q+B_2\Delta Q+M_4K_{iE}\Delta e_E+M_4K_{iQ}\Delta e_{nQ}\end{cases} \tag{18}$$

where $M_1=diag\left(\left[m_{11}\ \cdots\ m_{1n}\right]^T\right)$, $M_2=diag\left(\left[m_{21}\ \cdots\ m_{2n}\right]^T\right)$,

$M_3=diag\left(\left[m_{31}\ \cdots\ m_{3n}\right]^T\right)$, $M_4=diag\left(\left[m_{41}\ \cdots\ m_{4n}\right]^T\right)$,

$N_d=diag\left(\left[n_{d1}\ \cdots\ n_{dn}\right]^T\right)$, $N_q=diag\left(\left[n_{q1}\ \cdots\ n_{qn}\right]^T\right)$,

$A_1=-M_2\left(I_n+K_{pE}L_E\right)$, $A_2=-M_2\left(I_n+K_{pQ}L_Q\right)N$, $B_1=-M_4\left(I_n+K_{pE}L_E\right)$,

$B_2=-M_4\left(I_n+K_{pQ}L_Q\right)N$, $\Delta E_d=\left[\Delta E_{d1}\ \cdots\ \Delta E_{dn}\right]^T$,

$\Delta E_q=\left[\Delta E_{q1}\ \cdots\ \Delta E_{qn}\right]^T$, $\Delta\omega=\left[\Delta\omega_1\ \cdots\ \Delta\omega_n\right]^T$.

In addition, considering the active power droop control and the low-pass filter effect

$$\Delta\dot{\omega}=-\omega_c\Delta\omega-\omega_cM\Delta p \tag{19}$$

where $M=diag\left(\left[m_1\ \cdots\ m_n\right]^T\right)$ is the *P-f* droop gain and $\Delta p=\left[\Delta p_1\ \cdots\ \Delta p_n\right]$ is instant active power.

B. Small-Signal Model for the Whole System

Considering load and line impedances together, the conductance matrix G and susceptance matrix B can be written as

$$G=\begin{bmatrix}G_{11}&\cdots&G_{1n}\\ \vdots&\ddots&\vdots\\ G_{n1}&\cdots&G_{nn}\end{bmatrix}, B=\begin{bmatrix}B_{11}&\cdots&B_{1n}\\ \vdots&\ddots&\vdots\\ B_{n1}&\cdots&B_{nn}\end{bmatrix} \tag{20}$$

Based on the *KCL* and *KVL* theorem, the small-signal model representing the relationship between output current and voltage can be written as

$$\begin{cases}\Delta I_d=G\Delta E_d+(-B)\Delta E_q\\ \Delta I_q=B\Delta E_q+G\Delta E_d\end{cases} \tag{21}$$

where $\Delta I_d=\left[\Delta I_{d1}\ \cdots\ \Delta I_{dn}\right]^T$, $\Delta I_q=\left[\Delta I_{q1}\ \cdots\ \Delta I_{qn}\right]^T$.

Since instant active and reactive powers are obtained through an orthogonal system as

$$\begin{cases}p_i=3/2\left(E_{di}I_{di}+E_{qi}I_{qi}\right)\\ q_i=3/2\left(E_{qi}I_{di}-E_{di}I_{qi}\right)\end{cases} \tag{22}$$

The small-signal model of the instant output power is presented as

$$\begin{cases} \Delta p = 3/2\left(I_d\Delta E_d + I_q\Delta E_d + E_d\Delta I_d + E_q\Delta I_q\right) \\ \Delta q = 3/2\left(-I_q\Delta E_d + I_d\Delta E_d + E_q\Delta I_d - E_d\Delta I_q\right) \end{cases} \tag{23}$$

where $I_d = diag\left(\left[I_{d1} \quad \cdots \quad I_{dn}\right]^T\right)$, $I_q = diag\left(\left[I_{q1} \quad \cdots \quad I_{qn}\right]^T\right)$,

$E_d = diag\left(\left[E_{d1} \quad \cdots \quad E_{dn}\right]^T\right)$, $E_q = diag\left(\left[E_{q1} \quad \cdots \quad E_{qn}\right]^T\right)$.

By combining (21) and (23), the small signal model of the instant active and reactive powers can be expressed as

$$\begin{cases} \Delta p = S_1\Delta E_d + S_2\Delta E_q \\ \Delta q = S_3\Delta E_d + S_4\Delta E_q \end{cases} \tag{24}$$

where $S_1 = 3/2\left(I_d + E_dG + E_qB\right)$, $S_2 = 3/2\left(I_q - E_dB + E_qG\right)$,

$S_3 = 3/2\left(-I_q + E_qG - E_dB\right)$, $S_4 = 3/2\left(I_d - E_qB - E_dG\right)$.

By substituting (24) into (11) and (19), and by substituting (15) into (7) and combining with (8) and (18), we can obtain the whole system model as follows

$$\dot{X} = FX \tag{25}$$

where $F = \begin{bmatrix} -\omega_c I_n & -\omega_c MS_1 & -\omega_c MS_1 & 0_n & 0_n & 0_n \\ M_1 & A_1N_d & A_1N_q & A_2 & M_2K_{iE} & M_2K_{iQ} \\ M_3 & B_1N_d & B_1N_q & B_2 & M_4K_{iE} & M_4K_{iQ} \\ 0_n & \omega_c S_3 & \omega_c S_4 & -\omega_c I_n & 0_n & 0_n \\ 0_n & -L_E^{'}N_d & -L_E^{'}N_q & 0_n & 0_n & 0_n \\ 0_n & 0_n & 0_n & -LQ_N & 0_n & 0_n \end{bmatrix}$,

$X = \left[\Delta\omega^T \quad \Delta E_d^T \quad \Delta E_q^T \quad \Delta Q^T \quad \Delta e_E^T \quad \Delta e_{nQ}^T\right]^T$.

In order to make the modeling process more clearly, Fig. 8 shows the equivalent small signal model diagram for the proposed controller and the ac MG system.

C. Stability Analysis

In order to analyze the model quantitatively, a MG including four parallel connected DGs, a local load and a common load are considered as a study case. In this Subsection, root locus plots are shown to reflect the dynamical behavior of the system by considering different control parameters.

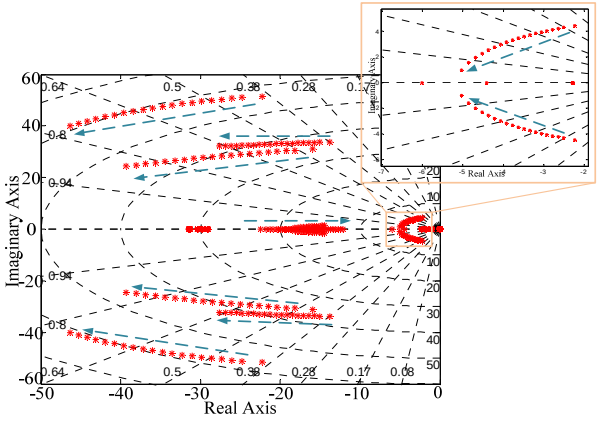

Fig. 9. Root locus plot 7<K_{pE}<15.

Fig. 9 shows the root locus movement considering the proportional coefficient K_{pE} of *PI* controller for containment-based control changing from 7 to 15. From the enlarged part in Fig. 9, it is shown that the two dominating poles located near the imaginary axis are moving towards the real axis and away from the imaginary axis, which indicate that the system is becoming more damped. Six complex poles which are also affected by K_{pE}, are moving away from the imaginary axis, thus improving the response speed.

Fig. 10 shows root locus considering integral coefficient K_{iE} of the *PI* controller for containment-based control changing from 1 to 100. From the enlarged part in Fig. 10, it is shown that two dominating poles are moving away from the real axis, which means that the system is becoming less damped. Simultaneously, two poles on the real axis are moving away from original point. The rest six complex poles are less affected than this last of proportional coefficient K_{pE}.

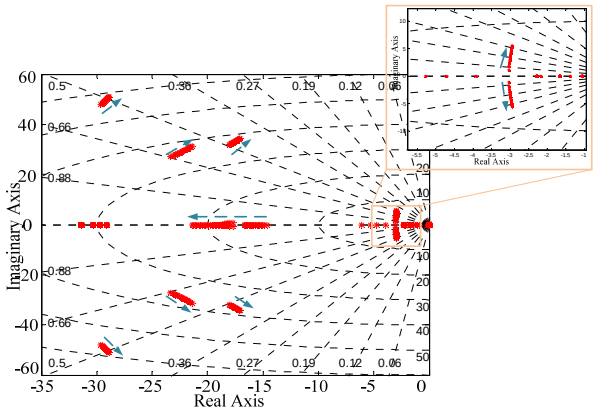

Fig. 10. Root locus plot 1<K_{iE}<100

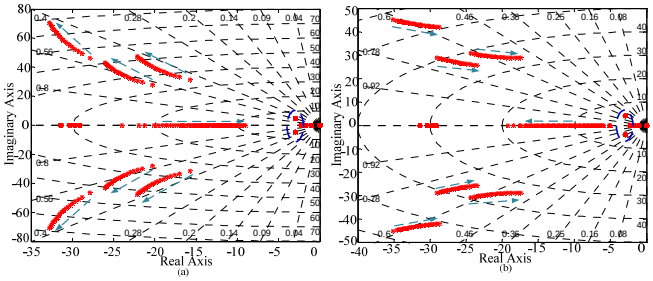

Fig. 11. Root locus: (a) 7<K_{pQ}<15; (b) 30<K_{iQ}<120.

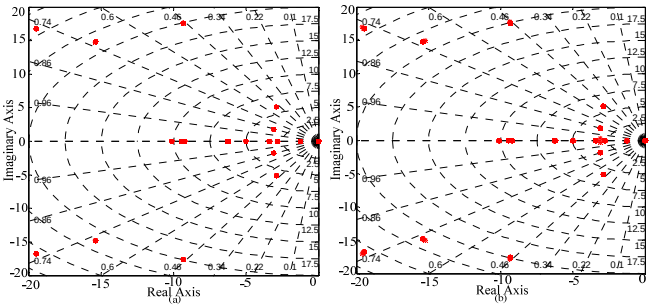

Fig. 12. Root locus: (a) Public Load from *(15+15.7j)Ω* to *(1500+1570j)Ω*; (b) Local Load from *(30+31.4)Ω* to *(3000+3140j)Ω*.

Fig. 11 (a) shows root locus considering proportional coefficients K_{pQ} for a *PI* controller for consensus-based control changing from 7 to 15. It can be observed that two dominating poles in the blue circle are barely affected. In addition, one pole on the real axis moves towards origin point, which can slow down the response speed. Six complex poles are moving away from real axis, which means the system is becoming less damped. Fig. 11 (b) shows root locus considering integral coefficients K_{iQ} of *PI* controller for consensus-based control changing from 30 to 120. The two dominating poles in the blue circle are also not affected. One dominating pole on the real

axis is moving away from the original point, which can increase the system response speed. Six complex poles are moving towards the imaginary axis which makes the system be less damped.

Figs. 12(a) and (b) show that the eigenvalues are not affected by load changes, including common and local loads, indicating good robustness of the proposed controllers. Thus, the proposed scheme does not require prior knowledge of the load information in the system. To be clearer, the whole analysis conclusion is summarized in Table I.

TABLE I. Conclusion from Stability Analysis

Containment-based Controller			Consensus-based Controller		
$\uparrow K_{pE}$	Response speed	$\uparrow$	$\uparrow K_{pQ}$	Response speed	$\downarrow$
	Damping	$\uparrow$		Damping	$\downarrow$
$\uparrow K_{iE}$	Response speed	---	$\uparrow K_{iQ}$	Response speed	$\uparrow$
	Damping	$\downarrow$		Damping	$\downarrow$

The analyses shown in Figs. 9-12 are based on the complete system information including the line impedance values which are difficult to know in real MG system. The root locus plots by changing the line impedance values from 0.8 to 1.2 times of the real values are shown in Fig. 13. It is shown that by changing the line impedance values cannot affect the poles much that from the control parameters. The result can also be derived by comparing the ranges of imaginary and real axis shown in Fig. 13, and that in Figs. 9-12. Thus, the parameter analysis method and results can be used for real MG system design without knowing the accurate value of line impedances. The values of the line impedances for this analysis are given in Table II.

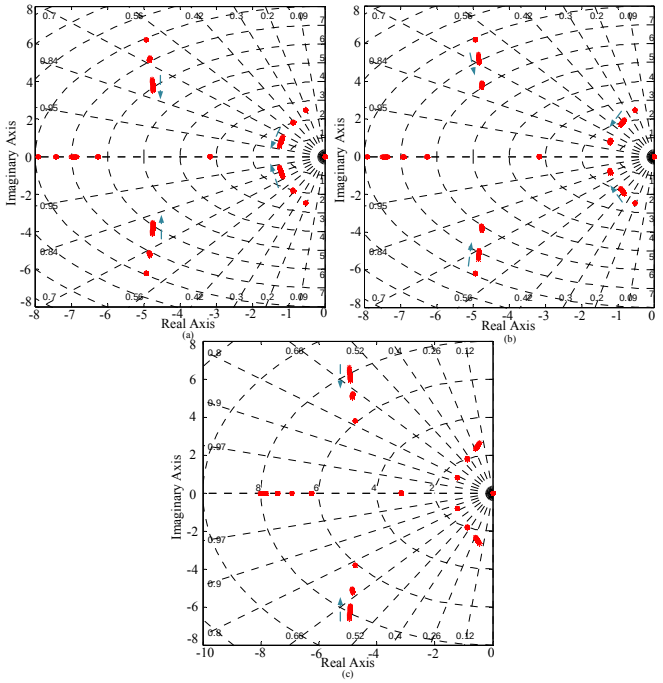

Fig. 13. Root locus: (a). Changing from $0.8*Z_{12}$ to $1.2*Z_{12}$; (b). Changing from $0.8*Z_{23}$ to $1.2*Z_{23}$; (c). Changing from $0.8*Z_{34}$ to $1.2*Z_{34}$.

V. Experimental Results

The proposed control scheme is implemented and tested in an experimental MG setup operating in islanded mode, shown in Fig. 14 at the AAU-Microgrid Research Laboratory. The setup consists of four parallel-configured power electronics inverters, a real-time control and monitor platform, LCL filters and RL loads. Communication link is only built between neighboring units shown in the top left corner of Fig. 13. Converters rated active and reactive power are 2: 2: 1: 1 for DG_1-DG_4. The nominal voltage magnitude is set to 325 V with 1% voltage boundary $(325 \pm 1\%)$. The experimental results are shown in Figs. 14-18. At t=*T0*, four DGs are controlled by the conventional droop control, and at t=*T1* the proposed controller is enabled.

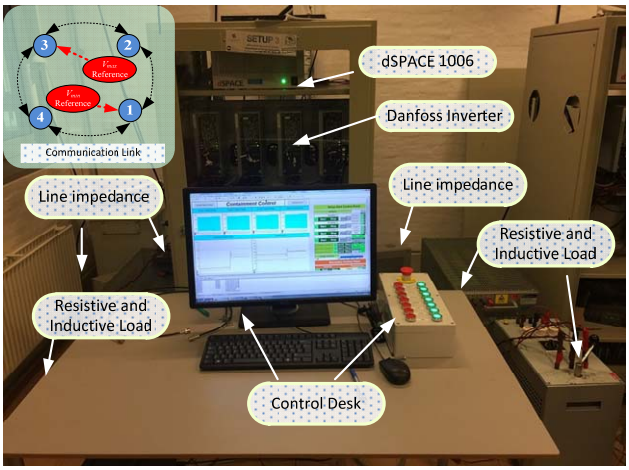

Fig. 14. Experimental setup in AAU-Microgrid research laboratory

A. Case 1: Performance Assessment and Comparison

Fig. 15 shows the performance comparison between the conventional droop controller and the proposed one. Fig. 15(a) shows the voltage performance and Fig. 15(b) shows the reactive power sharing characteristic. Before t=*T1*, the system is controlled by the conventional droop controller. The bus voltage magnitudes are dropped more than 18*V*, which exceed the lower voltage boundary 320*V*. The reactive power sharing among four DGs are not following the proportionality 2:2:1:1. At t=*T1*, the proposed controller is activated. Then, the bus voltage magnitudes can be bounded within prescribed range and the reactive power is proportionally shared to 2:2:1:1. Furthermore, between t=*T2* and t=*T4*, the boundary is changed and the bus voltage magnitudes are followed the changed boundary into the new range which is between 320*V* and 310*V*. In addition, the performance of reactive power sharing can also be guaranteed, being still equal to 2:2:1:1.

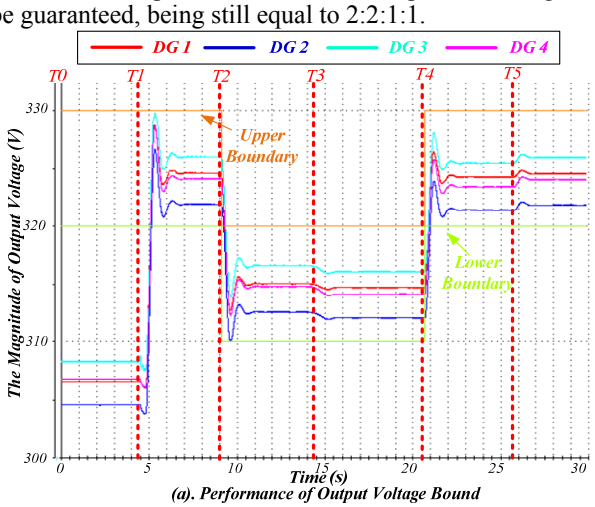

(a). Performance of Output Voltage Bound

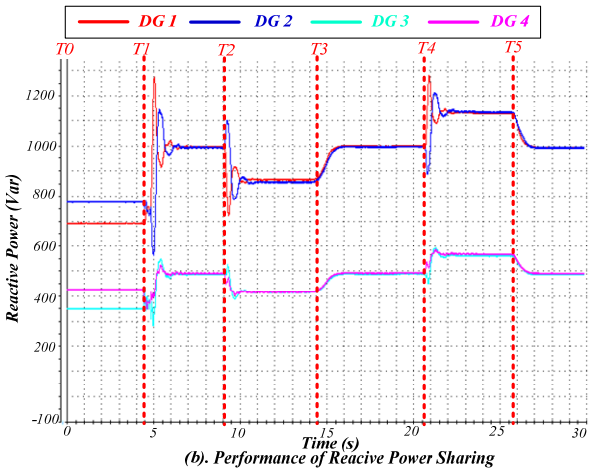

Fig. 15. Performance evaluation of the proposed controller

In addition, at t=*T3*, the load is changed and the performance of reactive power sharing is also kept accurate. After t=*T4*, the voltage boundary is changed back to the nominal range and both the voltage and reactive power sharing performance are kept well. It is shown that after activating the proposed controller, the bus voltage magnitudes can be bounded within the dynamic range. Meanwhile the output reactive power can be proportionally shared to 2:2:1:1 during the whole process.

B. Case 2: Communication Failure Resiliency

Resiliency to a single communication link failure is studied in Fig. 16.

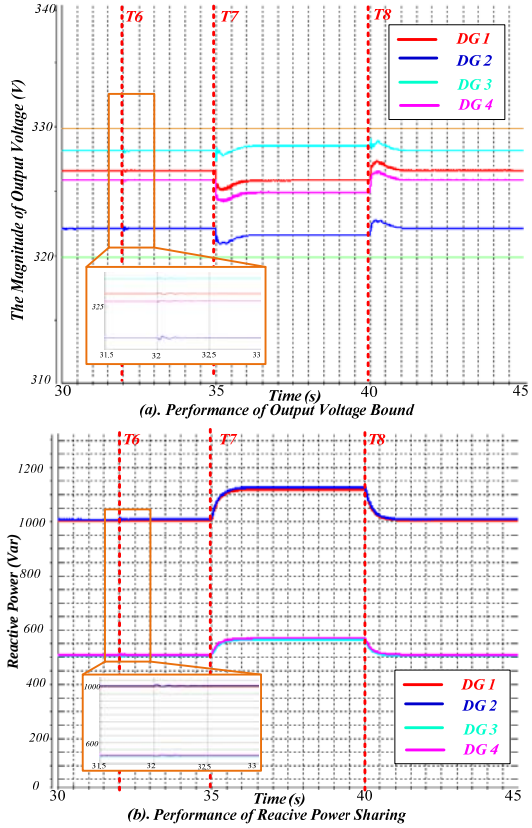

Fig. 16. Resiliency to communication failure Between DG_2 and DG_3

The communication link between DG_2 and DG_3 has been disabled at t=*T6*. As shown in the zoomed in part of Fig. 16(a) and (b), after small oscillations occur around $\pm 0.5V$, it does not have any impact on the performance of bounded bus voltage and reactive power sharing. After that, the load is switched at t=*T7* and *T8*. The performance is also kept well. It is concluded that both the dynamic and steady-state performance of the proposed controller cannot be affected as long as the communication network remains connected from the perspective of graph theory.

C. Case 3: Plug-and-Play Comparison Study

Fig. 17 studies the plug-and-play capability of the proposed controller. DG_4 is unplugged at t=*T9*. Thus, the bus voltage and reactive power from DG_4 decay to zero. Notice that a source failure also means loss of communication links connected to other DGs. As shown in Fig. 17(a), the bus voltages of DG_1-DG_3 are kept inside the acceptable range. In addition, Fig. 17(b) shows the per-unit value of output reactive power to decrease the range of *y*-axis, indicating that the per-unit values of output reactive power among DG_1-DG_3 are all equals to $0.55p.u.$ At t=*T10*, DG_4 begin to synchronize the frequency and phase with the MG. After successful synchronization, at t=*T11*, DG_4 is connected without activating the proposed controller. At t=*T12*, the proposed controller and communication are activated for DG_4. Fig. 17 shows that bus voltage magnitudes can be bounded within the range and the per-unit value of reactive power sharing among four DGs are equal to $0.47p.u.$ after activating the proposed controller for DG_4.

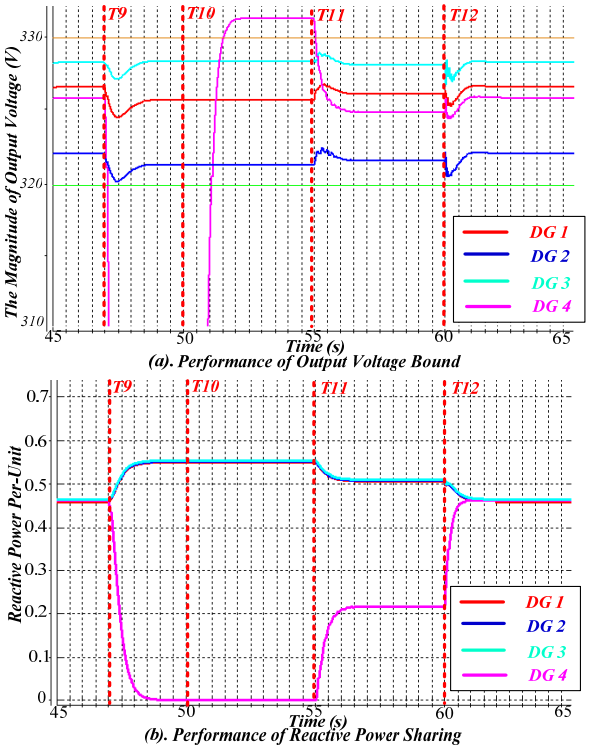

Fig. 17. Plug-and-Play Study for DG_4 under proposed controller.

Furthermore, to make the proposed containment-based voltage controller more convincing, the control performance by using controllers of [17] and [19], which are very popular in the literature about voltage and reactive power sharing regulation, are shown in Figs. 18-19 by using the same electrical topology respectively.

Fig. 18 shows the plug-and-play performance of the controller proposed in [17]. When DG_4 is disconnected from the MG, the bus voltage of DG_2 exceeds the voltage boundary which can affect the power quality of the system. In addition, as shown in Fig. 19, by using the controller proposed in [19], when DG_4 is plugged out of the system, even though the average voltage value can be kept at $325V$, shown in Fig. 19(c), the bus voltage of DG_2 also exceeds the voltage boundary shown in Fig. 19(a).

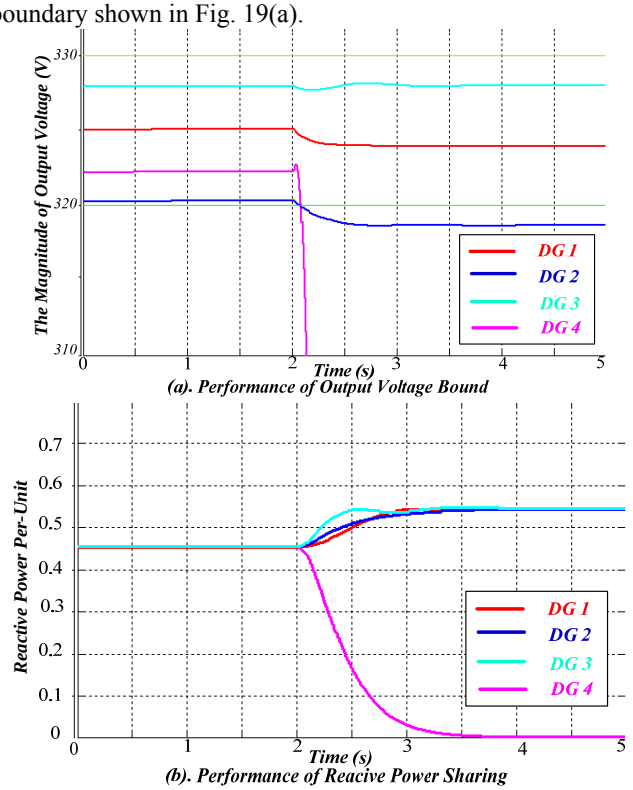

Fig. 18. Plug-and-Play Study for DG 4 under controller in [17].

Notice that the plug-and-play tests are also shown in [17] and [19] without observing this problem. The reason is that by comparing the electrical parameters of this paper with the ones in [17] and [19], the line impedance deviations that we use in this paper are much larger, and thus the total reactive power as well. The electrical data comparison is shown in Table II in detail. Thus, it is proved that the proposed containment-based controller is more suitable for larger systems with relatively larger line impedance deviations and higher reactive power sharing requirements.

TABLE II. Electrical Data Comparison

Category	In this paper	In Ref. [17]	In Ref. [19]
Line Impedance	Z_{12}=1.2Ω+5.4mH Z_{23}=0.4Ω+1.8mH Z_{34}=0.8Ω+3.6mH	Z_{12}=0.8Ω+3.6mH Z_{23}=0.4Ω+1.8mH Z_{34}=0.7Ω+1.9mH	Z_{12}=0.8Ω+3.6mH Z_{23}=0.4Ω+1.8mH Z_{34}=0.7Ω+1.5mH
Nominal Voltage	325 V	325 V	120 V
Total Reactive Power	3000 W	1260 W	750 W

Remark 1: If the line impedance deviations in the system are much higher and some DGs are disconnected of the system, it is not possible to guarantee both the performance of bus voltages bound and reactive power sharing simultaneous due to the electrical limitations. Under these conditions, the advantage of proposed controller is that it can decide either to guarantee the bus voltage bound through setting error saturation of reactive power sharing performance, or to guarantee the reactive power sharing performance through enlarging the voltage boundary of the system according to the MGs or electrical distribution standards. Previously proposed controllers cannot perform this high level of freedom to achieve global bus voltage bound, so that the control performance of all global voltages in the system cannot be compromised among DGs, especially under extreme conditions.

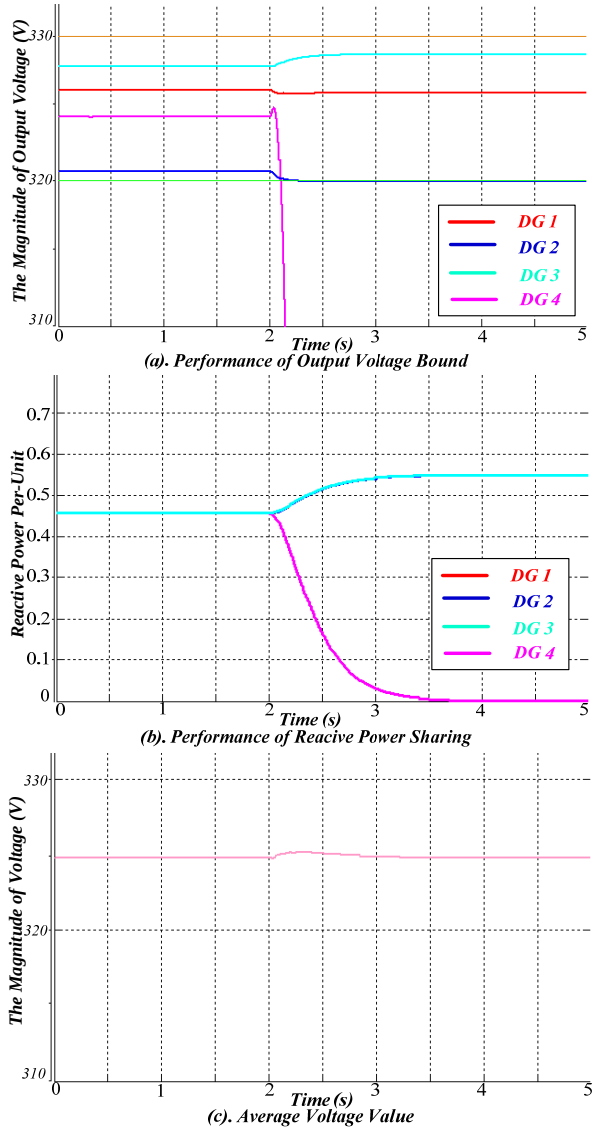

Fig. 19. Plug-and-Play Study for DG 4 under controller in [19].

VI. Conclusion

This paper presents the coupling/trade-off effects between voltage regulation and reactive power sharing in different levels of a hierarchical control structure. The coupling effects among Q-V droop gains, line impedance differences, reactive power sharing errors, and voltage magnitudes deviations are analyzed in the primary control level. The trade-off effects between the accurate reactive power sharing and voltage magnitudes regulations are further analyzed in the secondary level. A fully distributed coordination controller including both

containment-based and consensus-based controllers is proposed to offer a highly flexible and reliable operation of DGs, thus achieving both bound the voltage magnitudes within a reasonable range and achieving accurate reactive power sharing. A detailed small signal model is derived and the effects of different parameters change for the proposed controller are analyzed. Experimental results are presented to demonstrate the effectiveness of proposed controller including performance assessment and comparison, resiliency for communication failure and plug-and-play study.

REFERENCES

[1]. DOE Microgrid Workshop Report, U.S. Dept. Energy, San Diego, CA, USA, Aug. 2011.

[2]. J. M. Guerrero, J. C. Vasquez, J. Matas, M. Castilla, L. G. D. Vicuna, and M. Castilla, "Hierarchical control of droop-controlled ac and dc microgrids—A general approach toward standardization," *IEEE Trans. Ind. Electron*., vol. 58, no. 1, pp. 158-172, Jan. 2011.

[3]. L. Meng, A. Luna, E. Diaz, B. Sun, T. Dragicevic, M. Savaghebi, J. Vasquez, J. Guerrero, M. Graells, "Flexible System Integration and Advanced Hierarchical Control Architectures in the Microgrid Research Laboratory of Aalborg University," *IEEE Trans. Ind. Appl.*, vol. 52, no. 2, pp.1736-1749, Mar/Apr. 2016

[4]. M. C. Chandorkar, D. M. Divan, and R. Adapa, "Control of parallel connected inverters in standalone AC supply systems," *IEEE Trans. Ind. Appl*., vol. 29, no. 1, pp. 136-143, Jan./Feb. 1993.

[5]. R. Han, L. Meng, J. M. Guerrero, Q. Sun, J. C. Vasquez. "Coupling/tradeoff analysis and novel containment control for reactive power, output voltage in islanded Micro-Grid," 42nd Annual Conference of the IEEE Industrial Electronics Society, 2016.

[6]. Y. Li, C. Kao, "An accurate power control strategy for power-electronics-interfaced distributed generation units operating in a low-voltage multibus microgrid," *IEEE Trans. Power Electron*., vol. 24, no. 12, pp. 2977-2988, Dec. 2009.

[7]. H. Mahmood, D. Michaelson, J. Jiang, "Accurate reactive power sharing in an islanded microgrid using adaptive virtual impedances," *IEEE Trans. Power Electron.*, vol. 30, no. 3, pp. 1605-1617, Mar. 2015.

[8]. Y. Zhu, F. Zhuo, F. Wang, B. Liu, R. Gou, Y. Zhao, "A virtual impedance optimization method for reactive power sharing in networked microgrid," *IEEE Trans. Power Electron*., vol. 31, no. 4, pp. 2890-2904, Apr. 2016.

[9]. A. Jadbabaie, J. Lin, and A. S. Morse, "Coordination of groups of mobile autonomous agents using nearest neighbor rules," *IEEE Trans. Autom. Control,* vol. 48, no. 6, pp. 988–1001, Jun. 2003

[10]. K. Moore and D. Lucarelli, "Decentralized adaptive scheduling using consensus variables," *International Journal of Robust and Nonlinear Control*, vol. 17, no. 10-11, pp. 912-940, Jul. 2007.

[11]. R. Olfati-Saber and R. M. Murray, "Consensus problems in networks of agents with switching topology and time-delays," *IEEE Trans. Autom. Control*, vol. 49, no. 9, pp. 1520–1533, Sep. 2004.

[12]. R. Olfati-Saber, J. A. Fax, and R. M. Murray, "Consensus and cooperation in networked multi-agent systems," *Proc. IEEE*, vol. 95, no. 1. Pp. 215-233, Jan. 2007.

[13]. M. Ji, G. Ferrari-Trecate, M. Egerstedt, and A. Buffa, "Containment control in mobile networks," *IEEE Trans. on Automatic Control*, vol. 53, no. 8, pp. 1972–1975, Sep. 2008.

[14]. S. Qobad, J. M. Guerrero, J. C. Vasquez, "Distributed Secondary Control for Islanded MicroGrids - A Novel Approach," *IEEE Trans. on Power Electron.*, vol. 29, no. 2, pp. 1018-1031, Feb. 2014.

[15]. A. Milczrek, M. Malinowski, J. M. Guerrero, "Reactive power management in islanded microrid – Proportional power sharing in hierarchical droop control," *IEEE Trans. on Smart Grid.*, vol. 6, no. 4, pp. 1631-1638, Jul. 2015.

[16]. A. Bidram, A. Davoudi, F. L. Lewis, and J. M. Guerrero, "Distributed cooperative secondary control of microgrids using feedback linearization," *IEEE Trans. Power Syst*., vol. 28, no. 3, pp. 3462–3470, Aug. 2013.

[17]. J. W. Simpson-Porco, Q. Shafiee, F. Dorfler, J. C. Vasquez, J. M. Guerrero, F. Bullo, "Secondary Frequency and Voltage Control of Islanded Microgrids via Distributed Averaging," *IEEE Trans. Ind. Electron.*, vol. 58, no. 1, pp. 7025-7038, Nov. 2016.

[18]. L. Meng, *X. Zhao, F. Tang, M. Savaghebi, T. Dragicevic, J. C. Vasquez, J. M. Guerrero,* "Distributed Voltage Unbalance Compensation in Islanded Microgrids by Using a Dynamic Consensus Algorithm," *IEEE Trans. on Power Electron.*, vol. 31, no. 1, pp. 827-838, Jan. 2016.

[19]. V. Nasirian, Q. Shafiee, J. M. Guerrero, F. L. Lewis, A. Davoudi, "Droop-free distributed control for AC microgrid," *IEEE Trans. on Power Electron*., vol. 31, no. 2, pp. 1600-1617, Feb. 2016.

[20]. L. Meng, T. Dragicevic, J. Roldán-Pérez, J. C. Vasquez and J. M. Guerrero, "Modeling and Sensitivity Study of Consensus Algorithm-Based Distributed Hierarchical Control for DC Microgrids," *IEEE Trans. on Smart Grid*, vol. 7, no. 3, pp. 1504-1515, May 2016.

[21]. R. Han, L. Meng, G. F. Trecate, E. A. A. Coelho, J, C. Vasquez, J. M. Guerrero, "Containment and consensus-based distributed coordination control for voltage bound and reactive power sharing in AC microgrid," *IEEE Conference of Applied Power Electron*., APEC, pp. 3549-3556, 2017.

[22]. IEEE Draft Guide for Design, Operation, and Integration of Distributed Resource Island Systems with Electric Power Systems, *IEEE Standard P1547 Draft 4*.

[23]. M. Ji, G. Ferrari-Trecate, M. Egerstedt, and A. Buffa, "Containment control in mobile networks," *IEEE Trans. on Autom. Control*, vol. 53, no. 8, pp. 1972–1975, Sep. 2008.

[24]. P. Kunder, Power System Stability and Control. New York, NY, USA: McGraw-Hill, 1994